



Solubility of difluoromethane (R-32) and pentafluoroethane (R-125) in 1-alkyl-3-methylimidazolium tricyanomethanide ionic liquids

Miguel Viar, Salvador Asensio-Delgado, Fernando Pardo, Gabriel Zarca, Ane Urtiaga*

Department of Chemical and Biomolecular Engineering, Universidad de Cantabria, Av. Los Castros 46, Santander 39005, Spain

ARTICLE INFO

Keywords:

Absorption
Hydrofluorocarbon
Ionic liquid
NRTL
Phase equilibrium
Vapor-liquid equilibrium

ABSTRACT

The recovery of refrigerant blends and the subsequent separation of value-added hydrofluorocarbons (HFCs) for reuse would help to meet the phase-down in the production of virgin HFCs established by the Kigali Amendment to the Montreal Protocol. The use of ionic liquids (ILs) in extractive distillation processes has become particularly relevant. In this process, the selection of the IL is the core element for a technically and economically feasible design. For this purpose, the absorption of the HFCs difluoromethane (R-32) and pentafluoroethane (R-125), components of the equimassic mixture R-410A, in 1-alkyl-3-methylimidazolium tricyanomethanide ILs was studied. The isochoric saturation method was applied to report vapor-liquid equilibrium data over a temperature range of 283.15–323.15 K and up to 0.9 MPa. These data were fitted accurately to the NRTL activity coefficient model and the Henry's law constants, the activity coefficients at infinite dilution, the enthalpies and entropies of solvation and the thermodynamic mixing properties were calculated. Finally, [C₂C₁im][tcm] ranked as one of the most selective ILs to date, exhibiting a good R-32 absorption capacity that could make it a valuable solvent for the separation of R-410A by extractive distillation.

1. Introduction

Refrigeration systems enable the thermal comfort of society and are essential for industrial production and preservation of food and medicines [1]. In fact, the installed cooling capacity is expected to increase about 4–5 times by 2050 [2]. However, the most commonly used refrigeration equipment predominantly uses hydrofluorocarbons (HFCs) as working fluids for its operation. HFCs are synthetic compounds that exhibit global warming potentials (GWP) up to 10,000 times higher than CO₂. Moreover, their emissions doubled in 2014 compared to 1990, and it is estimated that if decisive action is not taken, they could account for up to 20 % of total GHG emissions by 2050 [3,4]. For this reason, a gradual reduction of the consumption and production of HFCs with high GWP has been implemented through international agreements and regulations, highlighting the pioneering Regulation EU 517/2014 and the Kigali Amendment to the Montreal Protocol. These regulations have established a paradigm shift in the refrigeration sector, defining the term 'reclamation', that is, the reprocessing of a fluorinated greenhouse gas, recovered during maintenance or prior to disposal, to match the equivalent performance of a virgin substance [5]. For recycling purposes, the azeotropic or near-azeotropic behavior of refrigerant mixtures

hinders the separation of the abated blends into their components so that they can be reused in new refrigerant blends together with low-GWP hydrofluoroolefins (HFOs) and hydrocarbons (HCs). To that end, several technologies are being developed, namely, adsorption on porous materials [6–8], membrane separation [9–12], and extractive distillation processes [13–16]. The latter relies on the selective absorption of HFCs in liquid entrainers, among which some ionic liquids (ILs) have acquired special relevance due to their unique properties, namely, negligible vapor pressure, wide liquid temperature range, thermal and chemical stability, and high sorption capacity for HFCs [17].

The design of IL-based extractive distillation separations requires accurate knowledge on the solubility of HFCs into ILs. Asensio-Delgado et al. [4] recently published a review of the progress made this far, including more than 4,000 vapor-liquid equilibrium points for more than 190 absorption pairs formed by 52 ILs and 26 different fluorinated refrigerants. However, this field of research is still experiencing a continuous growth boosted by the restrictions imposed on the production of virgin HFCs, and novel solubility data in ILs are being reported [18–22]. Moreover, the search and analysis of the best IL entrainer is being complemented with quantum chemistry [23–25], molecular dynamics [18,26–28] and artificial neural network [29,30] approaches.

* Corresponding author.

E-mail address: urtiaga@unican.es (A. Urtiaga).

Our research group has focused on the solubility assessment of some of the most common HFCs and HFOs, namely, difluoromethane (R-32), 1,1,1,2-tetrafluoroethane (R-134a), pentafluoroethane (R-125), trans-1,3,3,3-tetrafluoropropene (R-1234yf) and 1,3,3,3-tetrafluoropropene (R-1234ze(E)), into low-viscosity ILs that exhibit high solubility selectivity for the challenging separation of refrigerant mixtures such as R-32/R-125, R-134a/R-1234yf and R-134a/R-1234ze(E) [17,18,31,32]. In these works, we found that nitrile-based ILs offer an excellent platform to perform the extractive distillation of refrigerant mixtures because of their low viscosity and high solubility selectivity. The solubility of fluorinated hydrocarbons in these ILs increases with the number of nitrile groups, from thiocyanate- to dicyanamide- and tricyanomethanide-based ILs, which is coupled to a slight decrease in the observed solubility selectivity. Particularly, Asensio-Delgado et al. [18] determined the solubility of R-134a, R-1234yf and R-1234ze(E) in imidazolium-based ILs with the tricyanomethanide anion ([C_nC₁im][tcm], n: 2,4,6,8) with special interest on understanding the different solubility behavior of the HFO isomers R-1234yf and R-1234ze(E) through molecular dynamic simulations. This work complements the previous study by assessing the solubility data of R-32 and R-125, the components of the widely used refrigerant R-410A, in the same family of tricyanomethanide-based ILs and evaluating their potential separation with these ILs.

2. Experimental section

2.1. Materials

The refrigerants R-32 and R-125 were supplied by Coproven Climatización (Gas Servei licensed supplier, Spain). The ILs 1-ethyl-3-methylimidazolium tricyanomethanide ([C₂C₁im][tcm]), 1-butyl-3-methylimidazolium tricyanomethanide ([C₄C₁im][tcm]), 1-hexyl-3-methylimidazolium tricyanomethanide ([C₆C₁im][tcm]), and 1-octyl-3-methylimidazolium tricyanomethanide ([C₈C₁im][tcm]) were purchased from IoLiTec (Germany) at 98 wt% purity and vacuum-dried for 24 h at 333.15 K to remove any traces of water prior to use. Table 1 collects the specifications of the chemicals used. The final water content was measured to be lower than 50 ppm using a coulometric Karl-Fischer titration method (899 Coulometer, Metrohm, ±1 ppm).

2.2. Experimental procedure and solubility measurement

The isochoric saturation method was used to evaluate the solubility of the refrigerant gases in the selected ILs. The experimental system consisted of an absorption chamber and a storage cylinder connected by a valve, as it was described and validated in previous works [17,31,32]. Briefly, the absorption chamber was a jacketed stirred tank reactor (Buchi, Picoclave model, 170 mL), equipped with a pressure transducer (Keller, PAA-33X series, 0.01 % accuracy) and a Pt-100 temperature sensor connected to a thermostatic bath (Julabo, F25-ME model, ±0.01 K). The storage cylinder (140 mL) was equipped with another pressure transducer.

The absorption chamber was loaded with 30 g (±0.0001 g) of IL, ensuring that the volume of gas introduced is larger enough than the loaded IL, minimizing the effect of volumetric expansion of the IL during

gas absorption [17]. Prior to each experiment, the IL was kept at 333.15 K under vacuum for at least 12 h to remove any dissolved traces of water and volatile compounds. Then, after adjusting the working temperature, a certain amount of gas was introduced into the storage cylinder and the pressure and temperature were recorded. Later, the valve was opened and both phases came into contact in the absorption chamber. The stirrer was set to 500 rpm to accelerate the absorption, and pressure and temperature were continuously recorded until the equilibrium was reached, that is, when the pressure remained constant for more than 20 min. This experimental procedure was validated in our previous works with available VLE data for CO₂ and other F-gas/systems [32].

The solubility was calculated from the temperature and pressure measurements as the mole fraction of gas dissolved in the liquid phase:

$$x = \frac{n_{abs}}{n_l + n_{abs}} \quad (1)$$

where n_{abs} are the total moles of gas dissolved and n_l are the moles of IL loaded into the cell. Each absorption isotherm consisted of various consecutive absorption steps, where the total gas absorbed in each step (n_i) was determined as follows:

$$n_i = \rho_{i,S} \cdot V_S + \rho_{i-1,C} \cdot (V_C - V_i) - \rho_{i,eq} \cdot (V_S + V_C - V_i) \quad (2)$$

where V_S , V_C and V_i are the volumes of the storage cylinder, the absorption chamber, and the loaded IL, and $\rho_{i,S}$, $\rho_{i-1,C}$ and $\rho_{i,eq}$ are the gas molar densities in the storage cylinder, in the absorption chamber, and at the equilibrium, respectively. From the experimental measurements of temperature and pressure, the molar densities were calculated by using the Peng-Robinson cubic equation of state to account for deviations from the ideal behavior. The total amount of gas dissolved was calculated as the amount absorbed in each step plus the amount dissolved in the previous stages (n_k):

$$n_{abs} = n_i + \sum_{k=1}^{i-1} n_k \quad (3)$$

Once the solubility data were determined, the Henry's law constants (k_H) were calculated from:

$$k_H(T) = \lim_{x \rightarrow 0} \frac{\bar{f}(P, T)}{x} \quad (4)$$

where \bar{f} is the refrigerant gas fugacity calculated using the Peng-Robinson equation of state. To determine the limit at infinite dilution, the experimental solubility was fitted to a second order polynomial [26, 35].

The solubility uncertainty was calculated using the quadratic expansion of error, expanding each variable until considering all the measured properties (i.e., temperature, pressure, and mass). In particular, the uncertainty in molar fraction was determined as follows:

$$u(x) = \sqrt{\left(\frac{\partial x}{\partial n_{abs}}\right)^2 \cdot (u(n_{abs}))^2 + \left(\frac{\partial x}{\partial n_l}\right)^2 \cdot (u(n_l))^2} \quad (5)$$

For the Henry's law constants and the solvation properties, the uncertainty was calculated following the rigorous least squares adjustment as explained by Wentworth [36].

Table 1
Chemicals used in this work.

Chemical	CAS No.	Supplier	Fraction purity	Viscosity at 298 K (mPa·s)	Purification method	Water content (ppm)
[C ₂ C ₁ im][tcm]	666823-18-3	IoLiTec	>98 wt%	14.6 [33]	Vacuum dry	<50
[C ₄ C ₁ im][tcm]	878027-73-7	IoLiTec	>98 wt%	27.9 [33]	Vacuum dry	<50
[C ₆ C ₁ im][tcm]	1365535-17-6	IoLiTec	>98 wt%	41.0 [34]	Vacuum dry	<50
[C ₈ C ₁ im][tcm]	1203710-60-4	IoLiTec	>98 wt%	60.0 [34]	Vacuum dry	<50
R-32	75-10-2	Gas Servei, S.A.	>99.9 vol%	–	–	–
R-125	354-33-6	Gas Servei, S.A.	>99.9 vol%	–	–	–

3. Results and discussion

3.1. R-32 and R-125 solubility in [C_nC₁im][tcm] ILs

The experimental vapor-liquid equilibrium (VLE) data determined over the temperature range 283.15–323.15 K and pressures up to 0.9 MPa are presented in Tables 2–5 for each of the ILs under study. In addition, Figs. 1 and 2 represent the experimental and calculated isotherms for each refrigerant/IL pair.

The solubility data were modeled using the Non-Random Two-Liquid (NRTL) activity coefficient model, which has been widely applied in previous works of the field [37,38]. The VLE of each component of a mixture is described as follows:

$$y_i p \Phi_i = x_i \gamma_i p_i^S \quad (i \in \mathbb{Z} [1, N]) \tag{6}$$

where y_i , x_i are the molar fractions of the species i in the vapor and liquid phase, respectively, γ_i is the activity coefficient, p_i^S is the vapor pressure, and Φ_i , the Poynting correction factor. The latter was determined by:

$$\Phi_i = \exp \left[\frac{(B_i - V_i^L) \cdot (p - p_i^S)}{R \cdot T} \right] \tag{7}$$

where B_i is the second virial coefficient, V_i^L is the saturated liquid molar volume, and R is the ideal gas constant. The parameters p_i^S , B_i , and V_i^L were calculated using the CoolProp 6.4.0 [39] software, which implements multiparameter Helmholtz-energy-based equations of state that are specifically developed for each refrigerant. The combination of Eqs. (6) and (7) allows calculating the experimental activity coefficients considering that $y_{IL} = 0$ due to the negligible vapor pressure of ILs.

For a binary mixture, the NRTL activity coefficients were calculated as follows:

Table 2
Mole-fraction solubility of R-32 and R-125 in [C₂C₁im][tcm].*

T (K)	R-32			R-125		
	p (MPa)	x	u(x)	p (MPa)	x	u(x)
283.15	0.0410	0.0320	0.0003	0.0593	0.0106	0.0003
	0.1712	0.1267	0.0005	0.1811	0.0331	0.0005
	0.3519	0.2481	0.0006	0.3296	0.0622	0.0007
	0.4997	0.3420	0.0006	0.5252	0.1031	0.0010
293.15	0.6223	0.4178	0.0007	0.6914	0.1416	0.0013
	0.0416	0.0252	0.0003	0.0630	0.0083	0.0003
	0.1909	0.1096	0.0005	0.1851	0.0255	0.0005
	0.3944	0.2163	0.0006	0.3383	0.0477	0.0007
303.15	0.5644	0.2988	0.0007	0.5414	0.0783	0.0010
	0.7050	0.3645	0.0008	0.7151	0.1057	0.0014
	0.0481	0.0210	0.0003	0.0656	0.0070	0.0003
	0.2105	0.0928	0.0005	0.1914	0.0204	0.0005
313.15	0.4346	0.1846	0.0007	0.3474	0.0371	0.0008
	0.6188	0.2550	0.0008	0.5579	0.0592	0.0011
	0.7730	0.3113	0.0009	0.7340	0.0777	0.0015
	0.0578	0.0215	0.0003	0.0677	0.0051	0.0003
323.15	0.2288	0.0815	0.0005	0.1952	0.0148	0.0005
	0.4685	0.1598	0.0007	0.3600	0.0269	0.0008
	0.6622	0.2192	0.0009	0.5296	0.0383	0.0011
	0.8205	0.2646	0.0011	0.7236	0.0500	0.0016
323.15	0.0575	0.0174	0.0003	0.0730	0.0033	0.0003
	0.2444	0.0699	0.0005	0.2027	0.0103	0.0005
	0.4955	0.1347	0.0008	0.3628	0.0180	0.0008
	0.7016	0.1833	0.0010	0.5399	0.0253	0.0011
	0.8606	0.2195	0.0012	0.7298	0.0309	0.0017

* The standard uncertainties are $u(T) = 0.01$ K, and $u(p) = 0.0001$ MPa. The standard uncertainties for molar fraction, $u(x)$, are presented in the table.

Table 3
Mole-fraction solubility of R-32 and R-125 in [C₄C₁im][tcm].*

T (K)	R-32			R-125		
	p (MPa)	x	u(x)	p (MPa)	x	u(x)
283.15	0.0437	0.0360	0.0004	0.0663	0.0154	0.0004
	0.1832	0.1434	0.0006	0.1791	0.0430	0.0006
	0.3757	0.2769	0.0007	0.3273	0.0809	0.0009
	0.5320	0.3773	0.0007	0.5173	0.1340	0.0012
293.15	0.6580	0.4557	0.0007	0.6815	0.1850	0.0015
	0.0463	0.0301	0.0004	0.0632	0.0112	0.0004
	0.2062	0.1263	0.0006	0.1780	0.0318	0.0006
	0.4228	0.2438	0.0007	0.3341	0.0611	0.0009
303.15	0.5952	0.3299	0.0008	0.5362	0.1002	0.0013
	0.7397	0.3986	0.0009	0.7111	0.1354	0.0017
	0.0504	0.0254	0.0004	0.0644	0.0088	0.0004
	0.2286	0.1105	0.0006	0.1844	0.0254	0.0006
313.15	0.4773	0.2170	0.0008	0.3395	0.0468	0.0009
	0.6498	0.2836	0.0009	0.5492	0.0760	0.0013
	0.8271	0.3484	0.0011	0.7281	0.0972	0.0018
	0.0550	0.0224	0.0004	0.0670	0.0066	0.0004
323.15	0.2313	0.0892	0.0007	0.1941	0.0188	0.0007
	0.4813	0.1746	0.0009	0.3514	0.0335	0.0010
	0.6783	0.2359	0.0011	0.5639	0.0510	0.0014
	0.8393	0.2831	0.0013	0.7440	0.0639	0.0020
323.15	0.0683	0.0194	0.0004	0.0705	0.0041	0.0004
	0.2573	0.0755	0.0007	0.1934	0.0119	0.0007
	0.5202	0.1450	0.0010	0.3584	0.0214	0.0010
	0.7181	0.1932	0.0012	0.5753	0.0316	0.0015
	0.8774	0.2281	0.0016	0.7563	0.0368	0.0021

* The standard uncertainties are $u(T) = 0.01$ K, and $u(p) = 0.0001$ MPa. The standard uncertainties for molar fraction, $u(x)$, are presented in the table.

Table 4
Mole-fraction solubility of R-32 and R-125 in [C₆C₁im][tcm].*

T (K)	R-32			R-125		
	p (MPa)	x	u(x)	p (MPa)	x	u(x)
283.15	0.0428	0.0336	0.0004	0.0581	0.0156	0.0004
	0.1885	0.1547	0.0006	0.1712	0.0485	0.0006
	0.3655	0.2848	0.0006	0.3139	0.0918	0.0008
	0.5168	0.3865	0.0007	0.4911	0.1499	0.0011
293.15	0.6396	0.4648	0.0007	0.7161	0.2318	0.0013
	0.0478	0.0337	0.0004	0.0629	0.0112	0.0004
	0.2014	0.1337	0.0006	0.1802	0.0377	0.0006
	0.3659	0.2305	0.0007	0.3286	0.0720	0.0009
303.15	0.5498	0.3277	0.0008	0.5259	0.1201	0.0012
	0.7076	0.4054	0.0008	0.6957	0.1636	0.0015
	0.0510	0.0274	0.0004	0.0642	0.0104	0.0004
	0.2172	0.1129	0.0006	0.1859	0.0312	0.0006
313.15	0.4463	0.2183	0.0008	0.3389	0.0577	0.0009
	0.6295	0.2950	0.0009	0.5436	0.0935	0.0013
	0.7843	0.3546	0.0010	0.6038	0.1038	0.0017
	0.0573	0.0247	0.0004	0.0681	0.0082	0.0004
323.15	0.1556	0.0667	0.0006	0.1933	0.0241	0.0006
	0.4313	0.1715	0.0008	0.3506	0.0428	0.0009
	0.6429	0.2433	0.0010	0.5282	0.0647	0.0013
	0.8062	0.2947	0.0012	0.7151	0.0872	0.0018
323.15	0.0590	0.0212	0.0004	0.0685	0.0058	0.0004
	0.2498	0.0841	0.0007	0.1961	0.0175	0.0006
	0.5384	0.1681	0.0009	0.3584	0.0315	0.0010
	0.7266	0.2181	0.0011	0.5733	0.0484	0.0014
	0.8814	0.2569	0.0014	0.7415	0.0591	0.0020

* The standard uncertainties are $u(T) = 0.01$ K, and $u(p) = 0.0001$ MPa. The standard uncertainties for molar fraction, $u(x)$, are presented in the table.

Table 5
Mole-fraction solubility of R-32 and R-125 in [C₈C₁im][tcm].*

T (K)	R-32			R-125		
	p (MPa)	x	u(x)	p (MPa)	x	u(x)
283.15	0.0561	0.0530	0.0005	0.0620	0.0214	0.0005
	0.2013	0.1775	0.0007	0.1715	0.0618	0.0007
	0.4179	0.3364	0.0007	0.3146	0.1159	0.0010
	0.5717	0.4376	0.0007	0.4950	0.1887	0.0012
	0.6913	0.5120	0.0008	0.6543	0.2590	0.0015
293.15	0.0458	0.0331	0.0005	0.0600	0.0166	0.0005
	0.2178	0.1504	0.0007	0.1772	0.0488	0.0007
	0.4339	0.2786	0.0008	0.3246	0.0904	0.0010
	0.6062	0.3697	0.0009	0.5216	0.1478	0.0014
	0.7488	0.4400	0.0010	0.6887	0.1980	0.0018
303.15	0.0485	0.0293	0.0005	0.0629	0.0125	0.0005
	0.2261	0.1266	0.0007	0.1853	0.0377	0.0008
	0.4673	0.2415	0.0009	0.3374	0.0694	0.0011
	0.6531	0.3216	0.0010	0.5437	0.1124	0.0015
	0.8051	0.3807	0.0012	0.7188	0.1490	0.0020
313.15	0.0539	0.0259	0.0005	0.0671	0.0095	0.0005
	0.2401	0.1083	0.0008	0.1927	0.0293	0.0008
	0.5007	0.2093	0.0010	0.3492	0.0538	0.0011
	0.6914	0.2746	0.0012	0.5605	0.0858	0.0016
	0.8457	0.3230	0.0014	0.7376	0.1117	0.0022
323.15	0.0702	0.0267	0.0005	0.0725	0.0081	0.0005
	0.2601	0.0930	0.0008	0.1986	0.0223	0.0008
	0.5237	0.1745	0.0011	0.3613	0.0398	0.0012
	0.7228	0.2303	0.0013	0.5730	0.0595	0.0017
	0.8795	0.2683	0.0017	0.7447	0.0704	0.0024

* The standard uncertainties are $u(T) = 0.01$ K, and $u(p) = 0.0001$ MPa. The standard uncertainties for molar fraction, $u(x)$, are presented in the table.

$$\ln(\gamma_1) = x_2^2 \left[\tau_{21} \cdot \left(\frac{G_{21}}{x_1 + x_2 \cdot G_{21}} \right)^2 + \frac{\tau_{12} \cdot G_{12}}{(x_2 + x_1 \cdot G_{12})^2} \right] \quad (8)$$

where

$$G_{12} = \exp(-\alpha \cdot \tau_{12}), \quad G_{21} = \exp(-\alpha \cdot \tau_{21}) \quad (9)$$

$$\tau_{12} = \tau_{12}^0 + \frac{\tau_{12}^1}{T}, \quad \tau_{21} = \tau_{21}^0 + \frac{\tau_{21}^1}{T} \quad (10)$$

The parameter α is an adjustable parameter, which was assumed to be constant and equal to 0.2 for fluorocarbons, in accordance with previous works reported in the literature [32,40]. Then, only the temperature-dependent binary interaction parameters τ_{12} and τ_{21} were optimized in this work as a function of two adjustable coefficients (Eq. (10)): τ_{12}^1 and τ_{21}^1 represent the excess Gibbs free energy divided by the ideal gas constant, while, τ_{12}^0 and τ_{21}^0 have no physical meaning and are only used to model systems with large deviations from the ideal behavior. Then, the NRTL activity coefficients (γ_{calc}) were modeled to fit the experimental values (γ_{exp}) by optimizing the binary interaction parameters in order to obtain the minimum average absolute relative deviation in activity coefficients (AARD, Eq. (11)) and pressure (AARD_p, Eq. (12)).

$$AARD = \frac{100}{N} \sum_{i=1}^N \left| \frac{\gamma_{exp} - \gamma_{calc}}{\gamma_{exp}} \right| \quad (11)$$

$$AARD_p = \frac{100}{N} \sum_{i=1}^N \left| \frac{P_{exp} - P_{calc}}{P_{exp}} \right| \quad (12)$$

Table 6 compiles the values of the NRTL parameters and deviations

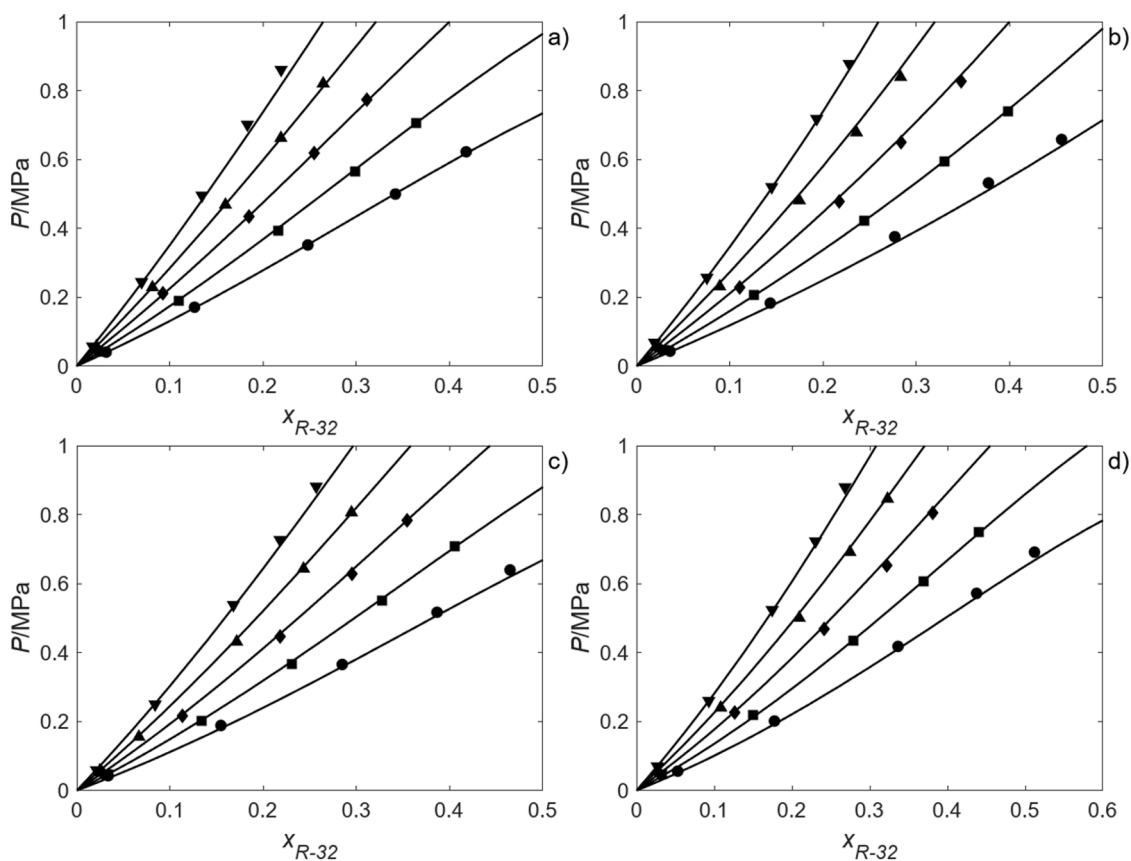


Fig. 1. Solubility of R-32 in a) [C₂C₁im][tcm], b) [C₄C₁im][tcm], c) [C₆C₁im][tcm], and d) [C₈C₁im][tcm] at different temperatures: 283.15 (●), 293.15 (■), 303.15 (◆), 313.15 (▲), and 323.15 K (▼). The solid lines represent the NRTL model calculations.

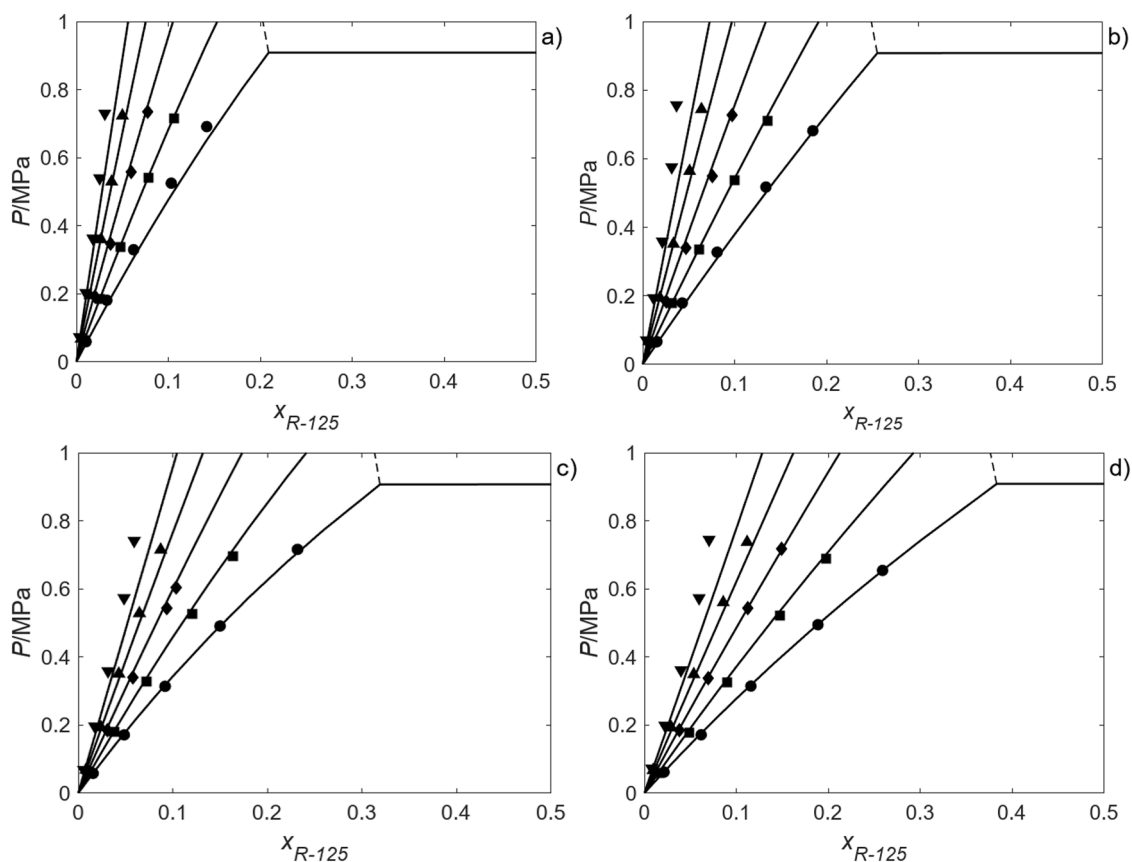


Fig. 2. Solubility of R-125 in a) [C₂C₁im][tcm], b) [C₄C₁im][tcm], c) [C₆C₁im][tcm], and d) [C₈C₁im][tcm] at different temperatures: 283.15 (●), 293.15 (■), 303.15 (◆), 313.15 (▲), and 323.15 K (▼). The solid lines represent the NRTL model calculations, and the dashed lines represent the immiscibility region predicted by the NRTL model.

Table 6

NRTL parameters for the solubility of R-32 and R-125 in [C_nC₁im][tcm] (n: 2, 4, 6, 8).

System	α	τ_{12}^0	τ_{12}^1 (K)	τ_{21}^0	τ_{21}^1 (K)	AARD (%)	AARD _p (%)
R-32 + [C ₂ C ₁ im][tcm]	0.2	0	1110.9	0	-427.18	1.31	1.38
R-125 + [C ₂ C ₁ im][tcm]	0.2	12.336	-316.46	4.3208	-1010.9	6.25	6.65
R-32 + [C ₄ C ₁ im][tcm]	0.2	0	5585.9	0	-49.938	2.53	2.67
R-125 + [C ₄ C ₁ im][tcm]	0.2	12.202	-316.85	4.0997	-1030.5	7.05	7.47
R-32 + [C ₆ C ₁ im][tcm]	0.2	0	1087.8	0	-473.98	2.19	2.28
R-125 + [C ₆ C ₁ im][tcm]	0.2	0	3899.4	0	212.14	5.87	6.22
R-32 + [C ₈ C ₁ im][tcm]	0.2	0	1163.4	0	-514.77	2.10	2.21
R-125 + [C ₈ C ₁ im][tcm]	0.2	0	4049.8	0	159.56	5.53	5.86

for each refrigerant/IL pair. As can be seen, the four NRTL binary parameters were only optimized for two systems in which the solubility of the HFC R-125 is low (particularly at the highest temperatures) in order to obtain an AARD lower than 10 %, while for all other systems the model results matched the experimental data with an error of less than 7 % with only two adjustable parameters. Furthermore, the NRTL activity coefficient model was also applied to predict the liquid-liquid equilibrium (LLE) of the refrigerant + IL mixtures following the procedure described in our previous works [17,18,32]. Thus, in Fig. 2, the immiscibility regions where the three phases (gas + IL with gas dissolved + liquefied gas) coexist are described with dashed lines. It is worth noting that, although there are no experimental data in this region, the immiscibility is predicted when the saturation pressures of the refrigerants are reached. Hence, the need to determine LLE data experimentally in order to validate the model prediction is highlighted.

Table 7 and Table 8 list the Henry's law constants for each pair R-32/

Table 7

Henry's law constants (MPa) of R-32.

Temperature (K)	IL			
	[C ₂ C ₁ im][tcm]	[C ₄ C ₁ im][tcm]	[C ₆ C ₁ im][tcm]	[C ₈ C ₁ im][tcm]
283.15	1.339 ± 0.018	1.247 ± 0.022	1.129 ± 0.016	1.068 ± 0.022
	293.15	1.694 ± 0.013	1.576 ± 0.016	1.416 ± 0.010
303.15	2.170 ± 0.012	1.951 ± 0.014	1.804 ± 0.008	1.668 ± 0.014
	313.15	2.719 ± 0.010	2.468 ± 0.015	2.228 ± 0.020
323.15	3.356 ± 0.020	3.108 ± 0.024	2.819 ± 0.025	2.569 ± 0.038

Table 8
Henry's law constants (MPa) of R-125.

Temperature (K)	IL			
	[C ₂ C ₁ im][tcm]	[C ₄ C ₁ im][tcm]	[C ₆ C ₁ im][tcm]	[C ₈ C ₁ im][tcm]
283.15	5.507 ± 0.030	4.210 ± 0.019	3.502 ± 0.019	2.797 ± 0.008
293.15	7.189 ± 0.018	5.590 ± 0.043	4.486 ± 0.016	3.671 ± 0.014
303.15	9.341 ± 0.051	6.989 ± 0.225	5.872 ± 0.035	4.843 ± 0.013
313.15	12.248 ± 0.214	9.546 ± 0.264	7.985 ± 0.156	6.194 ± 0.016
323.15	15.476 ± 0.953	12.477 ± 1.258	10.043 ± 0.315	7.607 ± 0.642

IL and R-125/IL, respectively. This thermodynamic parameter provides information on the solubility of the gas in the liquid at infinite dilution; the lower its value, the higher the solubility. Thus, the IL with the highest solubility is [C₈C₁im][tcm], followed by [C₆C₁im][tcm], [C₄C₁im][tcm] and [C₂C₁im][tcm]. These results are in good agreement with the trend describing the increase of refrigerant solubility with increasing IL molar volume reported in previous works [4,17]. More precisely, the longer alkyl chain of the cation provides more available free volume due to the lower cohesive energy attributed to the smaller contribution from the ionic groups [18], which eventually leads to a higher absorption capacity.

The thermodynamic properties of solvation were calculated from the Henry's law constants at infinite dilution using the van't Hoff equation:

$$\Delta H_{sol} = R \cdot \left(\frac{\partial \ln k_H}{\partial (1/T)} \right)_p \quad (13)$$

$$\Delta S_{sol} = -R \cdot \left(\frac{\partial \ln k_H}{\partial \ln T} \right)_p \quad (14)$$

The results, presented in Table 9, indicate that the HFC absorption is an exothermic process and enthalpically favorable which may be related with the gas-IL interactions. On the other hand, the absorption is entropically unfavorable. R-125, a bigger molecule than R-32, exhibits an entropy of solvation more negative than the R-32, which entails a less-ordered structure in solution leading to a lower gas solubility as it was shown previously. These results are in accordance with previous works [32,37,41].

Solubility differences can be also explained calculating the activity coefficients at infinite dilution (γ_1^∞), which are derived from the NRTL model (Eq. (8)) when $x_1 = 0$ and $x_2 = 1$:

$$\ln(\gamma_1^\infty) = \tau_{21} + \tau_{12} \cdot G_{12} \quad (15)$$

Table 10 presents the calculated γ_1^∞ for the systems under study. The attractive interactions between the dissolved solute and the solvent become stronger as γ_1^∞ decreases, thus the gas solubility increases. For both gasses, γ_1^∞ decreases as the alkyl chain length of the IL cation increases, following the same trend observed for the Henry's constants.

Table 9
Enthalpy and entropy of solvation of R-32 and R-125.

System	ΔH_{sol} (kJ·mol ⁻¹)	ΔS_{sol} (J·mol ⁻¹ ·K ⁻¹)
R-32 + [C ₂ C ₁ im][tcm]	-17.736 ± 0.002	-58.1 ± 0.8
R-125 + [C ₂ C ₁ im][tcm]	-19.109 ± 0.004	-64.8 ± 0.8
R-32 + [C ₄ C ₁ im][tcm]	-17.704 ± 0.007	-58.0 ± 1.4
R-125 + [C ₄ C ₁ im][tcm]	-19.653 ± 0.005	-67.0 ± 1.6
R-32 + [C ₆ C ₁ im][tcm]	-17.599 ± 0.005	-57.8 ± 1.0
R-125 + [C ₆ C ₁ im][tcm]	-19.107 ± 0.011	-64.7 ± 2.8
R-32 + [C ₈ C ₁ im][tcm]	-16.202 ± 0.005	-53.5 ± 1.2
R-125 + [C ₈ C ₁ im][tcm]	-19.609 ± 0.002	-65.9 ± 0.7

Table 10
Activity coefficients of R-32 and R-125 in [C_nC₁im][tcm] ILs at infinite dilution.

IL	Refrigerant	γ_1^∞				
		283.15 K	293.15 K	303.15 K	313.15 K	323.15 K
[C ₂ C ₁ im][tcm]	R-32	1.325	1.375	1.422	1.464	1.502
	R-125	6.963	7.825	8.727	9.665	10.637
[C ₄ C ₁ im][tcm]	R-32	1.228	1.286	1.347	1.411	1.477
	R-125	5.301	5.972	6.674	7.407	8.167
[C ₆ C ₁ im][tcm]	R-32	1.114	1.162	1.206	1.247	1.284
	R-125	5.083	5.227	5.375	5.526	5.678
[C ₈ C ₁ im][tcm]	R-32	0.989	1.039	1.087	1.131	1.173
	R-125	3.984	4.121	4.262	4.407	4.553

3.2. Mixing thermodynamic properties

To gain further insight into the absorption process, the mixing thermodynamic properties were evaluated. The absorption process operated isothermally can be divided into two phases: (i) the condensation of the gaseous solute, and (ii) the dissolution of the liquid solute in the solvent [21,42,43]. Then, the total enthalpy (ΔH_{total}) and entropy (ΔS_{total}) of the process are described as:

$$\Delta H_{total} = \Delta H_{cond} + \Delta H_{mix} \quad (16)$$

$$\Delta S_{total} = \Delta S_{cond} + \Delta S_{mix} \quad (17)$$

where ΔH_{cond} and ΔS_{cond} represents the condensation enthalpy and entropy, calculated with CoolProp 6.4.0. ΔH_{mix} and ΔS_{mix} are the mixing enthalpy and entropy of the dissolution of the liquid solute. Both parameters and the mixing Gibbs energy (ΔG_{mix}) are determined as follows:

$$\Delta H_{mix} = \Delta H^{id} + \Delta H^E \quad (18)$$

$$\Delta S_{mix} = \Delta S^{id} + \Delta S^E \quad (19)$$

$$\Delta G_{mix} = \Delta G^{id} + \Delta G^E \quad (20)$$

where ΔH^{id} , ΔS^{id} and ΔG^{id} are the thermodynamic properties for the ideal solution, and ΔH^E , ΔS^E and ΔG^E are the excess thermodynamic properties. The mixing properties for an ideal solution are calculated as:

$$\Delta H^{id} = 0 \quad (21)$$

$$\Delta S^{id} = R \cdot [x_1 \cdot \ln(x_1) + x_2 \cdot \ln(x_2)] \quad (22)$$

$$\Delta G^{id} = R \cdot T \cdot [x_1 \cdot \ln(x_1) + x_2 \cdot \ln(x_2)] \quad (23)$$

The molar excess properties are calculated as:

$$\Delta H^E = -R \cdot T^2 \cdot \left[x_1 \cdot \frac{\partial \ln(\gamma_1)}{\partial T} + x_2 \cdot \frac{\partial \ln(\gamma_2)}{\partial T} \right] \quad (24)$$

$$\Delta G^E = R \cdot T \cdot [x_1 \cdot \ln(\gamma_1) + x_2 \cdot \ln(\gamma_2)] \quad (25)$$

$$\Delta S^E = \frac{\Delta H^E - \Delta G^E}{T} \quad (26)$$

Tables S1–S8 shows the results obtained for each pair F-gas/IL evaluated in the Supplementary Information. The absorption of R-32 in the IL [C₈C₁im][tcm] presents the highest negative ΔG_{mix} values, resulting in a better absorption capacity and a stronger spontaneity compared to the other pairs. This phenomenon agrees with the results obtained experimentally, that is, ILs with higher alkyl chain present a higher absorption capacity, and the refrigerant gas R-32 is able to dissolve more easily than R-125 in ILs. This trend can also be checked with the ΔS_{mix} , where a higher value indicates a higher irreversibility of the dissolution of the solute. For R-32, the ΔS_{mix} values are positive for

all ILs, while for R-125, negative ΔS_{mix} values are presented, reflecting its low solubility. Finally, the reduction of solubility at increasing temperature can be observed in the ΔH_{total} and ΔS_{total} values, whose absolute values decrease with temperature.

3.3. Separation of R-32 and R-125 with ILs

The separation of the refrigerant mixtures R-410A into its components (R-32 and R-125) with ILs has been extensively evaluated through the simulation of extractive distillation processes. Viar et al. [14] reported that the solubility selectivity is the most critical design parameter to develop the separation process with low energy consumption and economic costs, with a stronger influence on the design than the absorption capacity. In the extractive distillation column, the IL preferentially absorbs R-32, and the R-125 becomes the major component in the distillate stream due to its poor solubility in most ILs. Hence, the ideal IL is the one that exhibits a high solubility selectivity, but also a great absorption capacity towards R-32 (low Henry's law constant). In this sense, Fig. 3 presents a comparison of the ILs for which VLE data at different temperatures and pressures are available, which is presented in terms of the ideal R-32/R-125 solubility selectivity (calculated as the ratio of the Henry's law constants) and the R-32 absorption capacity at 1 bar and 303.15 K (Eq. (27) [4]).

$$\text{Absorption capacity at 1 bar} \left(\frac{\text{mol gas}}{\text{L IL}} \right) = \frac{1}{(k_H - 1) \cdot V_m^L} \quad (27)$$

where V_m^L is the molar volume of the IL.

As can be seen, $[\text{C}_2\text{C}_1\text{im}][\text{SCN}]$ is the most selective IL for separating mixtures of R-32 and R-125, followed by $[\text{C}_2\text{C}_1\text{im}][\text{dca}]$ and $[\text{C}_2\text{C}_1\text{im}][\text{tcm}]$. Moreover, a selectivity decrease was observed with increasing the alkyl chain length, whereas the R-32 absorption capacity (expressed in mol per liter of IL) was not significantly affected for $[\text{dca}]^-$ and $[\text{TF}_2\text{N}]^-$ ILs or even decreased for the $[\text{tcm}]^-$ ILs. Overall, $[\text{tcm}]^-$ ILs stand as promising solvents for the separation of the R-410A mixture. With the exception of $[\text{C}_8\text{C}_1\text{im}][\text{tcm}]$, all of them show a solubility selectivity higher than $[\text{C}_4\text{C}_1\text{im}][\text{PF}_6]$, which was the reference IL used to date in extractive distillation processes for separating refrigerant blends [13,16,45]. In particular, $[\text{C}_2\text{C}_1\text{im}][\text{tcm}]$ showed only a slightly lower solubility selectivity than $[\text{C}_2\text{C}_1\text{im}][\text{SCN}]$ and $[\text{C}_2\text{C}_1\text{im}][\text{dca}]$, but a greater absorption capacity. Notwithstanding, it is a low-viscous IL (14.6 mPa·s at 298 K), whose improved absorption capacity together with the great solubility selectivity may show an excellent performance in the design of extractive distillation processes.

4. Conclusions

The solubility of R-32 and R-125, components of the widespread R-410A refrigerant mixture, was evaluated in four tricyanomethanide-based ILs, $[\text{C}_2\text{C}_1\text{im}][\text{tcm}]$, $[\text{C}_4\text{C}_1\text{im}][\text{tcm}]$, $[\text{C}_6\text{C}_1\text{im}][\text{tcm}]$, and $[\text{C}_8\text{C}_1\text{im}][\text{tcm}]$, at different temperatures and pressures. The phase behavior of the refrigerant/IL pairs were successfully modeled using the NRTL activity coefficient model with an AARD below 7 % in almost every case. The solubility differences between these two refrigerants in ILs were assessed based on the Henry's law constants, the activity coefficients at infinite dilution and the mixing thermodynamic properties, showing the higher solubility of R-32 with respect to R-125. The ILs proposed in this work also present high ideal selectivity in comparison with the ILs previously reported in the literature. More concretely, $[\text{C}_2\text{C}_1\text{im}][\text{tcm}]$ ranked as the third IL studied to date with the highest selectivity for the separation of the R-410A refrigerant blend. Therefore, given its good R-32 absorption capacity, $[\text{C}_2\text{C}_1\text{im}][\text{tcm}]$ stands as a promising solvent to be used in the separation of the R-410A blend by an extractive distillation process.

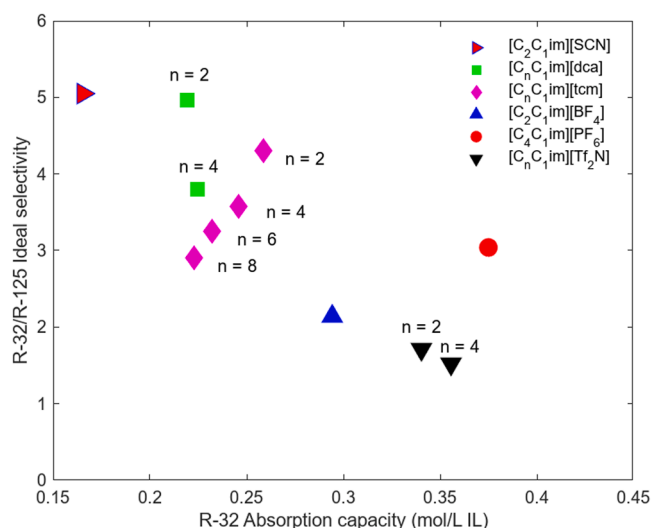


Fig. 3. Trade-off between R-32/R-125 solubility selectivity and R-32 absorption capacity at 303.15 K and 1 bar [17,31,35,37,44].

CRediT authorship contribution statement

Miguel Viar: Formal analysis, Investigation, Writing – original draft. **Salvador Asensio-Delgado:** Formal analysis, Software, Validation. **Fernando Pardo:** Methodology, Supervision. **Gabriel Zarca:** Conceptualization, Writing – review & editing, Supervision, Funding acquisition, Project administration. **Ane Urriaga:** Conceptualization, Writing – review & editing, Supervision, Funding acquisition, Project administration.

Declaration of Competing Interest

The authors declare that they have no known competing financial interests or personal relationships that could have appeared to influence the work reported in this paper.

Data availability

All data provided within the manuscript and supporting information.

Acknowledgements

The authors acknowledge the financial support of MCIN/AEI/10.13039/501100011033 and the European Union NextGenerationEU/PRTR to projects PID2019–105827RB-I00 and TED2021–129844B-I00. F. Pardo thanks the postdoctoral fellowship IJC2020–043134-I “Juan de la Cierva Incorporación”. M. Viar acknowledges the Concepción Arenal UC-22–23 pre-doctoral fellowship, funded by the University of Cantabria and the Government of Cantabria.

Supplementary materials

Supplementary material associated with this article can be found, in the online version, at doi:10.1016/j.fluid.2023.113983.

References

- [1] R. Khosla, N.D. Miranda, P.A. Trotter, A. Mazzone, R. Renaldi, C. McElroy, F. Cohen, A. Jani, R. Perera-Salazar, M. McCulloch, Cooling for sustainable development, *Nat. Sustain.* 4 (2021) 201–208, <https://doi.org/10.1038/s41893-020-00627-w>.

- [2] P.J. Castro, J.M.M. Araújo, G. Martinho, A.B. Pereira, Waste management strategies to mitigate the effects of fluorinated greenhouse gases on climate change, *Appl. Sci.* 11 (2021) 4367, <https://doi.org/10.3390/app11104367>.
- [3] N.D. Miranda, P. Giovanni Palafox-Alcantar, R. Khosla, M.D. McCulloch, Metrics for the emissions of F-gas refrigerants, *Sustain. Energy Technol. Assess.* 58 (2023), 103348, <https://doi.org/10.1016/j.seta.2023.103348>.
- [4] S. Asensio-Delgado, F. Pardo, G. Zarca, A. Urriaga, Absorption separation of fluorinated refrigerant gases with ionic liquids: equilibrium, mass transport, and process design, *Sep. Purif. Technol.* 276 (2021), 119363, <https://doi.org/10.1016/j.seppur.2021.119363>.
- [5] The European parliament and the council of the European union, regulation (EU) No 517/2014 of the European Parliament and of the Council of 16 April 2014 on fluorinated greenhouse gases and repealing Regulation (EC) No 842/2006, *Off. J. Eur. Union* 150 (2014) 195–230.
- [6] A.D. Yancey, D.R. Corbin, M.B. Shiflett, Difluoromethane (HFC-32) and Pentafluoroethane (HFC-125) Sorption on Linde Type A (LTA) Zeolites for the Separation of Azeotropic Hydrofluorocarbon Refrigerant Mixtures, *Langmuir* 38 (2022) 1937–1953, <https://doi.org/10.1021/acs.langmuir.1C02904>.
- [7] R.P.L. Ribeiro, J.E. Sosa, J.M. Araújo, A.B. Pereira, J.P. Mota, Vacuum swing adsorption for R-32 recovery from R-410A refrigerant blend, *Int. J. Refrig.* 150 (2023) 253–264, <https://doi.org/10.1016/j.ijrefrig.2023.01.020>.
- [8] A.B. Pereira, J.E. Sosa, R.P.P.L. Ribeiro, P.J. Castro, J.P.B. Mota, J.M.M. Araújo, Sorption of fluorinated greenhouse gases in silica-supported fluorinated ionic liquids, *J. Environ. Chem. Eng.* 10 (2022), 108580, <https://doi.org/10.2139/ssrn.4130037>.
- [9] A.N. Harders, E.R. Sturd, J.E. Vallier, D.R. Corbin, W.R. White, C.P. Junk, M. B. Shiflett, Selective separation of HFC-32 from R-410A using poly(dimethylsiloxane) and a copolymer of perfluoro(butenyl vinyl ether) and perfluoro(2,2-dimethyl-1,3-dioxole), *J. Memb. Sci.* 652 (2022), 120467, <https://doi.org/10.1016/j.memsci.2022.120467>.
- [10] F. Pardo, G. Zarca, A. Urriaga, Effect of feed pressure and long-term separation performance of Pebax-ionic liquid membranes for the recovery of difluoromethane (R32) from refrigerant mixture R410A, *J. Memb. Sci.* 618 (2021), 118744, <https://doi.org/10.1016/j.memsci.2020.118744>.
- [11] F. Pardo, S.V. Gutiérrez-Hernández, P. Rodríguez-San Miguel, G. Zarca, A. Urriaga, Polymer/ionic liquid pilot scale membrane prototype for the recovery of difluoromethane (R-32) from refrigerant mixtures, *Sep. Purif. Technol.* 320 (2023), 124115, <https://doi.org/10.1016/j.seppur.2023.124115>.
- [12] S.V. Gutiérrez-Hernández, F. Pardo, A.B. Foster, P.M. Budd, G. Zarca, A. Urriaga, Outstanding performance of PIM-1 membranes towards the separation of fluorinated refrigerant gases, *J. Memb. Sci.* 675 (2023) 1–9, <https://doi.org/10.1016/j.memsci.2023.121532>.
- [13] M.S. Monjur, A. Iftakher, M.M.F. Hasan, Separation process synthesis for high-GWP refrigerant mixtures: extractive distillation using ionic liquids, *Ind. Eng. Chem. Res.* 61 (2022) 4390–4406, <https://doi.org/10.1021/acs.iecr.2c00136>.
- [14] M. Viar, S. Asensio-Delgado, F. Pardo, G. Zarca, A. Urriaga, In the quest for ionic liquid entrainers for the recovery of R-32 and R-125 by extractive distillation under rate-based considerations, *Sep. Purif. Technol.* 324 (2023), 124610, <https://doi.org/10.1016/j.seppur.2023.124610>.
- [15] S. Asensio-Delgado, D. Jovell, G. Zarca, A. Urriaga, F. Llovel, Thermodynamic and process modeling of the recovery of R410A compounds with ionic liquids, *Int. J. Refrig.* 118 (2020) 365–375, <https://doi.org/10.1016/j.ijrefrig.2020.04.013>.
- [16] E.A. Finberg, M.B. Shiflett, Process designs for separating R-410A, R-404A, and R-407C using extractive distillation and ionic liquid entrainers, *Ind. Eng. Chem. Res.* 60 (2021) 16054–16067, <https://doi.org/10.1021/acs.iecr.1c02891>.
- [17] S. Asensio-Delgado, M. Viar, F. Pardo, G. Zarca, A. Urriaga, Gas solubility and diffusivity of hydrofluorocarbons and hydrofluoroolefins in cyanide-based ionic liquids for the separation of refrigerant mixtures, *Fluid Phase Equilib.* 549 (2021), 113210, <https://doi.org/10.1016/j.fluid.2021.113210>.
- [18] S. Asensio-Delgado, M. Viar, A.A.H. Pádua, G. Zarca, A. Urriaga, Understanding the molecular features controlling the solubility differences of R-134a, R-1234ze(E), and R-1234yf in 1-Alkyl-3-methylimidazolium tricyanomethanide ionic liquids, *ACS Sustain. Chem. Eng.* 10 (2022) 15124–15134, <https://doi.org/10.1021/acsuschemeng.2c04561>.
- [19] K.R. Baca, D.P. Broom, M.G. Roper, M.J. Benham, M.B. Shiflett, First measurements for the simultaneous sorption of difluoromethane and pentafluoroethane mixtures in ionic liquids using the integral mass balance method, *Ind. Eng. Chem. Res.* 61 (2022) 9774–9784, <https://doi.org/10.1021/acs.iecr.2c00497>.
- [20] K.R. Baca, G.M. Olsen, L. Matamoros Valenciano, M.G. Bennett, D.M. Haggard, B. J. Befort, A. Garciadiego, A.W. Dowling, E.J. Maginn, M.B. Shiflett, Phase equilibria and diffusivities of HFC-32 and HFC-125 in ionic liquids for the separation of R-410A, *ACS Sustain. Chem. Eng.* 10 (2022) 816–830, <https://doi.org/10.1021/acsuschemeng.1c06252>.
- [21] X. Jia, W. Dou, X. Wang, Solubility determination and mixing thermodynamic properties of R1243zf in two 1-butyl-3-methyl-imidazolium based ionic liquids, *J. Mol. Liq.* 364 (2022), 120031, <https://doi.org/10.1016/j.molliq.2022.120031>.
- [22] X. Jia, H. Wang, X. Wang, Solubility measurement, modeling and mixing thermodynamic properties of R1243zf and R600a in [BMIM][Ac], *J. Chem. Thermodyn.* 164 (2022), 106637, <https://doi.org/10.1016/j.jct.2021.106637>.
- [23] H. Qin, J. Cheng, H. Yu, T. Zhou, Z. Song, Hierarchical ionic liquid screening integrating COSMO-RS and aspen plus for selective recovery of hydrofluorocarbons and hydrofluoroolefins from a refrigerant blend, *Ind. Eng. Chem. Res.* 61 (2022) 4083–4094, <https://doi.org/10.1021/acs.iecr.1c04688>.
- [24] J.E. Sosa, R. Santiago, D. Hospital-Benito, M.C. Gomes, J.M.M. Araújo, A.B. Pereira, J. Palomar, Process evaluation of fluorinated ionic liquids as F-gas absorbers, *Environ. Sci. Technol.* 54 (2020) 12784–12794, <https://doi.org/10.1021/acs.est.0c05305>.
- [25] J.E. Sosa, R. Santiago, A.E. Redondo, J. Avila, L.F. Lepre, M.C. Gomes, J.M. M. Araújo, J. Palomar, A.B. Pereira, Design of ionic liquids for fluorinated gas absorption: COSMO-RS selection and solubility experiments, *Environ. Sci. Technol.* 56 (2022) 5898–5909, <https://doi.org/10.1021/acs.est.2c00051>.
- [26] L.F. Lepre, D. Andre, S. Denis-Quanquin, A. Gautier, A.A.H. Pádua, M.C. Gomes, Ionic liquids can enable the recycling of fluorinated greenhouse gases, *ACS Sustain. Chem. Eng.* 7 (2019) 16900–16906, <https://doi.org/10.1021/acsuschemeng.9b04214>.
- [27] N. Wang, Y. Zhang, K.S. Al-Barghouti, R. Kore, A.M. Scurto, E.J. Maginn, Structure and dynamics of hydrofluorocarbon/ionic liquid mixtures: an experimental and molecular dynamics study, *J. Phys. Chem. B* (2022) 8321, <https://doi.org/10.1021/acs.jpcc.2c05787>, 2022.
- [28] N. Wang, R.S. Defever, E.J. Maginn, Alchemical free energy and hamiltonian replica exchange molecular dynamics to compute hydrofluorocarbon isotherms in imidazolium-based ionic liquids, *J. Chem. Theory Comput.* 19 (2023) 3324–3335, <https://doi.org/10.1021/acs.jctc.3c00206>.
- [29] S. Asensio-Delgado, F. Pardo, G. Zarca, A. Urriaga, Machine learning for predicting the solubility of high-GWP fluorinated refrigerants in ionic liquids, *J. Mol. Liq.* 367 (2022), 120472, <https://doi.org/10.1016/j.molliq.2022.120472>.
- [30] J. Chu, Z. Zhang, X. Liu, M. He, Estimating the solubility of HFC/HFO in ionic liquids from molecular structure using machine learning method, *Chem. Eng. Res. Des.* 184 (2022) 315–325, <https://doi.org/10.1016/j.cherd.2022.06.015>.
- [31] S. Asensio-Delgado, F. Pardo, G. Zarca, A. Urriaga, Enhanced absorption separation of hydrofluorocarbon/hydrofluoroolefin refrigerant blends using ionic liquids, *Sep. Purif. Technol.* 249 (2020), 117136, <https://doi.org/10.1016/j.seppur.2020.117136>.
- [32] S. Asensio-Delgado, F. Pardo, G. Zarca, A. Urriaga, Vapor-liquid equilibria and diffusion coefficients of difluoromethane, 1,1,1,2-Tetrafluoroethane, and 2,3,3,3-tetrafluoropropene in low-viscosity ionic liquids, *J. Chem. Eng. Data* 65 (2020) 4242–4251, <https://doi.org/10.1021/acs.jced.0c00224>.
- [33] C.M.S.S. Neves, K. Adi Kurnia, J.A.P. Coutinho, I.M. Marrucho, J.N. Canongia Lopes, M.G. Freire, L.P.N. Rebelo, Systematic study of the thermophysical properties of imidazolium-based ionic liquids with cyano-functionalized anions, *J. Phys. Chem. B* 117 (2013) 10271–10283, <https://doi.org/10.1021/jp405913b>.
- [34] M. Musiał, S. Cheng, Z. Wojnarowska, M. Paluch, Density, viscosity, and high-pressure conductivity studies of tricyanomethanide-based ionic liquids, *J. Mol. Liq.* 317 (2020), 113971, <https://doi.org/10.1016/j.molliq.2020.113971>.
- [35] J.E. Sosa, R.P.P.L. Ribeiro, P.J. Castro, J.P.B. Mota, J.M.M. Araújo, A.B. Pereira, Absorption of fluorinated greenhouse gases using fluorinated ionic liquids, *Ind. Eng. Chem. Res.* 58 (2019) 20769–20778, <https://doi.org/10.1021/acs.iecr.9b04648>.
- [36] W.E. Wentworth, Rigorous least squares adjustment: application to some non-linear equations, II, *J. Chem. Educ.* 42 (1965) 162–167, <https://doi.org/10.1021/ed042p162>.
- [37] M.B. Shiflett, M.A. Harmer, C.P. Junk, A. Yokozeki, Solubility and diffusivity of difluoromethane in room-temperature ionic liquids, *J. Chem. Eng. Data* 51 (2006) 483–495, <https://doi.org/10.1021/je050386z>.
- [38] L. Dong, D. Zheng, G. Sun, X. Wu, Vapor-liquid equilibrium measurements of difluoromethane + [Emim]OTf, difluoromethane + [Bmim]OTf, difluoroethane + [Emim]OTf, and difluoroethane + [Bmim]OTf systems, *J. Chem. Eng. Data* 56 (2011) 3663–3668, <https://doi.org/10.1021/je2005566>.
- [39] I.H. Bell, J. Wronski, S. Quoilin, V. Lemort, Pure and pseudo-pure fluid thermophysical property evaluation and the open-source thermophysical property library coolprop, *Ind. Eng. Chem. Res.* 53 (2014) 2498–2508, <https://doi.org/10.1021/ie4033999>.
- [40] M.B. Shiflett, A. Yokozeki, Gaseous absorption of fluoromethane, fluoroethane, and 1,1,2,2-tetrafluoroethane in 1-butyl-3-methylimidazolium hexafluorophosphate, *Ind. Eng. Chem. Res.* 45 (2006) 6375–6382, <https://doi.org/10.1021/IE060192S>.
- [41] D.L. Minnick, M.B. Shiflett, Solubility and diffusivity of chlorodifluoromethane in imidazolium ionic liquids: [emim][Tf2N], [bmim][BF4], [bmim][PF6], and [emim][TFES], *Ind. Eng. Chem. Res.* 58 (2019) 11072–11081, <https://doi.org/10.1021/acs.iecr.9b02419>.
- [42] X. Jia, Y. Ma, X. Wang, Vapor-liquid equilibrium of 3, 3, 3-trifluoropropene with 1-ethyl-3-methyl-imidazolium tetrafluoroborate and 1-butyl-3-methyl-imidazolium tetrafluoroborate, *J. Mol. Liq.* 372 (2023), 121228, <https://doi.org/10.1016/j.molliq.2023.121228>.
- [43] Y. Sun, J. Wang, Q. Wei, X. Wang, Solubility for propane and isobutane in [p66614]cl from 278.15 to 348.15 K, *J. Chem. Eng. Data* 66 (2021) 1273–1279, <https://doi.org/10.1021/acs.jced.0c00901>.
- [44] X. Liu, M. He, N. Lv, X. Qi, C. Su, Vapor-liquid equilibrium of three hydrofluorocarbons with [HMIM][Tf2N], *J. Chem. Eng. Data* 60 (2015) 1354–1361, <https://doi.org/10.1021/je501069b>.
- [45] E.A. Finberg, T.L. May, M.B. Shiflett, Multicomponent refrigerant separation using extractive distillation with ionic liquids, *Ind. Eng. Chem. Res.* 61 (2022) 9795–9812, <https://doi.org/10.1021/acs.iecr.2c00937>.